ISSN 0915-633X

NATIONAL INSTITUTE FOR FUSION SCIENCE

Interpolated Differential Operator (IDO) Scheme for Solving Partial Differential Equations

T. Aoki

(Received - Aug. 22, 1996)

NIFS-449 Sep. 1996

RESEARCH REPORT
NIFS Series

This report was prepared as a preprint of work performed as a collaboration research of the National Institute for Fusion Science (NIFS) of Japan. This document is intended for information only and for future publication in a journal after some rearrangements of its contents.

Inquiries about copyright and reproduction should be addressed to the Research Information Center, National Institute for Fusion Science, Nagoya 464-01, Japan.

NAGOYA, JAPAN

Interpolated Differential Operator (IDO) Scheme for Solving Partial Differential Equations

Takayuki Aoki

Department of Energy Sciences, Tokyo Institute of Technology
4259 Nagatsuta, Midori-ku, Yokohama 226, Japan

abstract

We present a numerical scheme to apply to wide variety of partial differential equations (PDEs) in space and time. The scheme is based on high accurate interpolation of the profile for independent variables over a local area and repetitive differential operations by regarding PDEs as differential operators. We demonstrate that the scheme is applicable to all of hyperbolic, ellipsoidal and parabolic equations. The equations are solved in terms of the primitive independent variables, so that the scheme has flexibility for various type of equation including source terms. We find that the conservation holds accurate because of the high order scheme when we use a Hermite interpolation. The interface is found to be sharply described by adding an artificial viscosity term.

keywords : Partial Differential Equation, Hermite Interpolation, Non-conservative form, Numerical Scheme

1. Introduction

Most problems appearing in science and engineering are modeled by partial differential equations (PDEs) in space and time. The motivation to start this study was to construct an accurate approximation for local domain area by using the governing PDEs as efficiently as possible. We are able to make use of the equations derived by differentiating the given equation once or more. Since the domains are connected each other, we have a discretization scheme for initial boundary problems. When we have high accurate approximation profiles, we expect that an universal scheme will be obtained. We construct a high accurate interpolation on the discrete space to an approximate solution profile. The scheme presented in this paper consists of spatial

interpolation and multiple differential operations, and we call this scheme IDO (Interpolated Differential Operator).

For hyperbolic equations, many sophisticated schemes have been presented, for example TVD[1,2,3], ENO[4,5,6,7], PPM[8,9] and so on, and these obtain successfully good results for compressible fluid problems. These schemes solve the hyperbolic equations in a conservative form using flux correction. In this paper, we do not transform any independent variables into those taking account for the conservation or characteristics of the given equation. We take account for only flow direction. The given equations are solved for the primitive variables, so that for hyperbolic equations, the scheme becomes a non-conservative scheme. Although the scheme has a disadvantage for conservation, it makes possible to apply more flexibly to variation of PDEs, i.e., multicomponent flow[10] and including source terms. Recently CIP (Cubic Interpolated Propagation) scheme[11,12] has been presented, and applied to many problems[13,14,15]. In the CIP scheme, the spatial profile is described by a third order Hermite interpolation in the advection phase and updated by shifting the profile according to the local analytic solution. The CIP scheme for non-conservative form has been developed[16,17], and have results comparable with the best of conservative schemes.

A similar scheme DA-CIP with IDO has been presented by Utsumi[18]. The scheme applies a third order Hermite interpolation to the spatial derivative of the given equation. The time integration is split into two stages; fourth order Runge-Kutta integration and CIP advection. It is shown that hyperbolic equations are solved successfully. The Kond-P scheme[19] also uses Hermite interpolation to solve diffusion equation. In this paper, the IDO scheme also uses a Hermite interpolation, however, different kinds of interpolations are able to used if only they describe the higher derivatives enough accurately. A rational function[20] or hyper function are possible to be candidates.

This paper is organized as follows. In the next section, the basic concept of IDO scheme is illustrated in detail. For initial value problems, time-integration is also described. In section 3, the relation between CIP and IDO is discussed. Section 4 examines the accuracy of the IDO scheme by solving mass continuity equation and Poisson equation. In section 5, we apply IDO to various equations and the computational results are presented. In the final section, we give the conclusion and the subjects to study in the next paper.

2. Basic Concept

In this paper, we present a numerical scheme (Interpolated Differential Operator) IDO to solve hyperbolic, ellipsoidal and parabolic differential equations. The IDO scheme is constructed on the basis of discrete space (grid points) such as FDM, FEM and so on. The independent variables defined at the grid have a spatial profiles spreading over the local area which covers several grid points. The profile should approximate the solution of the governing PDE within the area. The IDO scheme requires a spatial interpolation enough accurate to describe high order spatial derivatives.

The given equations are solved in the original differential form described by the primitive independent variables. We regard the derivatives appearing in the equation as differential operators, and we can use the equations derived by temporal and spatial differentiation. We consider the following equation,

$$f_t = \mathfrak{I}_x f \,, \tag{1}$$

where the subscripts t and x denote time and spatial derivative operation, respectively. The symbol $\mathfrak{I}_x$ stands for a spatial differential operator. By taking time derivative of eq.(1), we have a series of the equations $f_{tt} = \mathfrak{I}_x \mathfrak{I}_x f$, $f_{ttt} = \mathfrak{I}_x \mathfrak{I}_x \mathfrak{I}_x f$, $\cdots$, and so on. Higher order time derivatives are also expressed by the spatial derivatives by successive operation of $\mathfrak{I}_x$. In the IDO scheme, the term $\mathfrak{I}_x f$ is not replaced by a finite difference expression, but $\mathfrak{I}_x$ operates the interpolation profile $F(x)$.

Most schemes for hyperbolic equation solve conservative form, however, the IDO solves it in the primitive form without any transformations of independent variables. Non-conservative form is applicable more flexibly to various kinds of differential equations with source terms.

2.1 Interpolation

In the IDO scheme, an independent variable has a spatial profile described by spatial interpolation covering several grid points. Various interpolations are possible if only they can describe spatial derivatives accurately, and in this paper we use a Hermite interpolation, which is determined by both the values and the derivatives. The Hermite interpolation has an enough accuracy, less computation and local interpolation area using neighboring grid information. We use two kinds of interpolation whose interpolated domain area are different.

Now we consider the i-th grid point and the interpolation function in one-dimension when the independent variables f and f_x have been given at all the grid points. In general, numerical information propagates in all the directions, so that the interpolation has to cover the area from $i-1$ to $i+1$. The Hermite interpolation is

obtained by the four matching conditions of $F(-\Delta x) = f_{i-1}$, $F_x(-\Delta x) = f_{x,i-1}$, $F(\Delta x) = f_{i+1}$, and $F_x(\Delta x) = f_{x,i+1}$. The coefficients of the fifth-order polynomial are determined as follows,

$$F(x) = a_c x^5 + b_c x^4 + c_c x^3 + d_c x^2 + f_{x,i} x + f_i \ , \tag{2}$$

$$a_c = -\frac{3}{4\Delta x^5}(f_{i+1} - f_{i-1}) + \frac{1}{4\Delta x^4}(f_{x,i+1} + 4f_{x,i} + f_{x,i-1}), \tag{2-1}$$

$$b_c = -\frac{1}{2\Delta x^4}(f_{i+1} - 2f_i + f_{i-1}) + \frac{1}{4\Delta x^3}(f_{x,i+1} - f_{x,i-1}), \tag{2-2}$$

$$c_c = \frac{5}{4\Delta x^3}(f_{i+1} - f_{i-1}) - \frac{1}{4\Delta x^2}(f_{x,i+1} + 8f_{x,i} + f_{x,i-1}), \tag{2-3}$$

$$d_c = \frac{1}{\Delta x^2}(f_{i+1} - 2f_i + f_{i-1}) - \frac{1}{4\Delta x}(f_{x,i+1} - f_{x,i-1}). \tag{2-4}$$

The higher derivatives more than f_x are obtained by differentiating the interpolation function with respect to x. At the i-th grid point, we have $f_{xx} = F_{xx}(0) = 2d_c$, $f_{xxx} = F_{xxx}(0) = 6c_c$, $f_{xxxx} = F_{xxxx}(0) = 24b_c$ and $f_{xxxxx} = 120a_c$, and higher derivatives are zero.

Another interpolation is used specially for advection term uf_x and their derived terms; for example, $f_t + uf_x = 0$. We call this upwind interpolation. When the advection velocity u is positive, the interpolation covers the area from i-1 to i-th grid. The interpolation function has the following third-order polynomial

$$F(x) = a_u x^3 + b_u x^2 + f_{x,i} x + f_i, \tag{3}$$

where the coefficients a_u and b_u are determined by the matching conditions of $F(-\Delta x) = f_{i-1}$, $F_x(-\Delta x) = f_{x,i-1}$, so that we have

$$a_u = \frac{(f_{x,i} + f_{x,i-1})}{\Delta x^2} - 2\frac{(f_i - f_{i-1})}{\Delta x^3}, \qquad b_u = \frac{(2f_{x,i} + f_{x,i-1})}{\Delta x} - 3\frac{(f_i - f_{i-1})}{\Delta x^2}. \tag{3-1}$$

In the case of $u < 0$, the interpolation covers the area from i to i+1-th grid, and the coefficients are derived by the condition of $F(\Delta x) = f_{i+1}$, $F_x(\Delta x) = f_{x,i+1}$ as follows,

$$a_u = \frac{(f_{x,i} + f_{x,i+1})}{\Delta x^2} + 2\frac{(f_i - f_{i+1})}{\Delta x^3}, \qquad b_u = -\frac{(2f_{x,i} + f_{x,i+1})}{\Delta x} - 3\frac{(f_i - f_{i+1})}{\Delta x^2}. \tag{3-2}$$

The higher derivatives more than f_x are obtained by taking derivative of the interpolation function as $f_{xx}(0) = F_{xx}(0) = 2b_u$ and $f_{xxx}(0) = 6a_u$ at the i-th grid point, and higher derivatives more than f_{xxx} are set to be zero.

In general, the derivative terms included in partial differential equations are classified into advection term and non-advection term, and the two kinds of interpolation are applied respectively.

2.2 Time advance

In the initial-value problem, time integration of the governing equation is done as

follows. We execute Taylor expansion for the independent variable with respect to time t, and we have an explicit scheme for time advance

$$f^{n+1} = f^n + f_t^n \Delta t + f_{tt}^n \frac{\Delta t^2}{2} + f_{ttt}^n \frac{\Delta t^3}{6} + O(\Delta t^4) \tag{4}$$

$$f_x^{n+1} = f_x^n + f_{tx}^n \Delta t + f_{ttx}^n \frac{\Delta t^2}{2} + f_{tttx}^n \frac{\Delta t^3}{6} + O(\Delta t^4) \tag{5}$$

where the superscripts $n+1$ and n mean the values of the time $t + \Delta t$ and t, respectively. The series of time derivative of f^n and f_x^n are replaced to the spatial derivative terms by using the given equation. We can select the order of the Taylor expansion, however, the order of spatial derivative is not able to exceed the order of the interpolated polynomial function. Moreover, there is the upper limit of the time interval Δt du to the numerical stability. In this paper, we no not discuss it, and we use Δt with which we found that the scheme is stable. On the other hand, we expand with respect to time $t + \Delta t$, we obtain the implicit formulation of time advance,

$$f^{n+1} = f^n + f_t^{n+1} \Delta t - f_{tt}^{n+1} \frac{\Delta t^2}{2} + f_{ttt}^{n+1} \frac{\Delta t^3}{6} + O(\Delta t^4) \tag{6}$$

$$f_x^{n+1} = f_x^n + f_{tx}^{n+1} \Delta t - f_{ttx}^{n+1} \frac{\Delta t^2}{2} + f_{tttx}^{n+1} \frac{\Delta t^3}{6} + O(\Delta t^4) \tag{7}$$

The numerical technique to solve eq.(6) and (7) depend on the governing equation, as is well known in the way of finite difference scheme.

3. Relation to the CIP scheme

Let consider the linear scalar equation $f_t = -uf_x$ with a constant advection velocity (u = const) as one of the simplest equations. The time derivatives f_t^n, f_{tt}^n and f_{ttt}^n for eq.(4) and f_{tx}^n, f_{ttx}^n and f_{tttx}^n for eq.(5) are required to update f^n and f_x^n at the grid point. Taking time-derivative and substituting $f_t = -uf_x$, we easily derive the series of the following equations

$$f_{tt} = u^2 f_{xx}, \quad f_{ttt} = -u^3 f_{xxx}, \quad f_{xtt} = -uf_{xx}, \quad f_{xtt} = u^2 f_{xxx}, \tag{8}$$

and so on. All the time derivatives are replaced by the spatial derivatives. When we apply the upwind interpolation (eq.(3)) to this problem, available highest derivative term is f_{xxx}^n, because the interpolation function is third-order polynomial. The time accuracy of the Taylor expansion becomes Δt^3 order. Substituting eqs.(8) into eq.(4) and eq.(5), we have

$$\begin{aligned} f^{n+1} &= f^n - u\Delta t f_x^n + \frac{(u\Delta t)^2}{2} f_{xx}^n - \frac{(u\Delta t)^3}{6} f_{xxx}^n \\ &= f^n - u\Delta t f_x^n + (u\Delta t)^2 b_u - (u\Delta t)^3 a_u \\ &= F(-u\Delta t), \end{aligned} \tag{9}$$

$$
\begin{aligned}
f_x^{n+1} &= f_x^n - u\Delta t\, f_{xx}^n + \frac{(u\Delta t)^2}{2} f_{xxx}^n \\
&= f_x^n - 2u\Delta t\, b_u + 3(u\Delta t)^2 a_u \\
&= F_x(-u\Delta t).
\end{aligned} \tag{10}
$$

It is found that the above two expressions are just the same as the procedure of the advection phase of CIP scheme[16,17], which makes use of the local analytic solution of advection equation; $f(t+\Delta t, x) = f(t, x-u\Delta x)$ and $f_x(t+\Delta t, x) = f_x(t, x-u\Delta x)$. When we substitute eqs.(8) into eq.(6) and (7), we have the implicit expression of the CIP scheme[21]. It concludes that the IDO scheme involves the CIP advection as a special case.

4. Accuracy of the IDO scheme

4.1 Mass Conservation

Since the IDO scheme becomes a non-conservative form in hyperbolic equation, it is useful to check the accuracy of conservation. We solve the following mass continuity equation,

$$\rho_t + (\rho u)_x = 0 \tag{11}$$

$$\rho_{tx} + (\rho u)_{xx} = 0 \tag{12}$$

with a steady and non-uniform velocity profile of $u = 1 + a\sin(k_x x)$, and $a = 0.25$. The higher derivatives are written down explicitly,

$$\rho_{tt} = -u\rho_{tx} - u_x\rho_t = u^2\rho_{xx} + 3uu_x\rho_x + (u_x^2 + uu_{xx})\rho \tag{13}$$

$$
\begin{aligned}
\rho_{ttx} &= -u\rho_{txx} - 2u_x\rho_{tx} - u_{xx}\rho_t \\
&= u^2\rho_{xxx} + 5uu_x\rho_{xx} + 4(u_x^2 + uu_{xx})\rho_x + (3u_xu_{xx} + uu_{xxx})\rho
\end{aligned} \tag{14}
$$

$$\rho_{ttt} = -u\rho_{ttx} - u_x\rho_{tt} \tag{15}$$

$$\rho_{tttx} = -u\rho_{ttxx} - 2u_x\rho_{ttx} - u_{xx}\rho_{tt} \tag{16}$$

where $\rho_{txx} = -(u\rho)_{xxx}$ and $\rho_{ttxx} = -(u\rho_t)_{xx}$ are used in eq.(14) and (16). We use the upwind interpolation for ρ_{xx} and ρ_{xxx}, and the analytic expression for the derivatives of the velocity. Time integration of Δt^3 order is done by substituting eqs.(11) ~ (16) into eq.(8) with $\Delta t = 0.4$. The results of total mass conservation $\int \rho dx$ is shown in Fig.1 as a function of the wave number k_x of the velocity profile. The initial density has a square profile; $\rho_i = 1$ for $7 \le i \le 27$ and $\rho_i = 0$ elsewhere. The total mass is integrated at the time t=200, and the mesh interval is $\Delta x = 1$. When we set $\rho_x = 0$ everywhere in the initial condition, the mass conservation error increases to 10^{-3} at the first time step, and it does not change by invisible rate. However, by setting $\rho_{x,6} = \rho_{x,7} = 0.5$ and $\rho_{x,27} = \rho_{x,28} = -0.5$ initially, we have the remarkably improved result. Figure 1 shows the deviation rate of IDO scheme from the initial mass, compared with the result of the

finite difference method (FDM) using non-conservative form of third-order upwind scheme as a reference. We use the following finite difference expression for third-order upwind scheme;

$$\rho_i^{n+1} = \rho_i^n - (u\overline{\rho}_x + \overline{u}_x\rho_i^n)\Delta t + \tfrac{1}{2}(u^2\overline{\rho}_{xx} + 3u\overline{u}_x\overline{\rho}_x + \overline{u}_{xx}\rho_i^n + \overline{u}_x^2\rho_i^n)\Delta t^2,$$

where

$$\overline{\rho}_x = (2\rho_{i+1}^n + 3\rho_i^n - 6\rho_{i-1}^n + \rho_{i-2}^n)/6\Delta x,$$
$$\overline{\rho}_{xx} = (-\rho_{i+2}^n + 16\rho_{i+1}^n - 30\rho_i^n - 16\rho_{i-1}^n - \rho_{i-2}^n)/12\Delta x^2,$$
$$\overline{u}_x = (-u_{i+2}^n + 8u_{i+1}^n - 8u_{i-1}^n + u_{i-2}^n)/12\Delta x^2$$
$$\overline{u}_{xx} = (-u_{i+2}^n + 16u_{i+1}^n - 30u_i^n - 16u_{i-1}^n - u_{i-2}^n)/12\Delta x^2.$$

It is found that the IDO scheme keeps quite good accuracy in spite of non-conservative form in spite of large nonuniformity of the advection velocity. The result of the CIP scheme stays in between IDO and FDM.

4.2 Spatial Accuracy

The spatial accuracy of the derivatives obtained by the interpolation can be estimated from the expressions (2) and (3). The accuracy of the numerical solution from the equation using the derivatives is not clear. Although there are many publications[16,17] of CIP using upwind Hermite interpolation, the scheme with use of the center Hermite interpolation has not been discussed enough[19]. In order to know the spatial accuracy of the numerical solution, we solve Poisson equation by IDO scheme.

For the independent variable f, we solve the original Poisson equation $f_{xx} = \phi$ using the center interpolation, where ϕ is the source term. For another independent variable f_x, we use the additional equation $f_{xxx} = \phi_x$ derived by taking derivative of the original equation. The explicit descriptions of the discrete formula are written down as follows,

$$\frac{2}{\Delta x^2}(f_{i+1} - 2f_i + f_{i-1}) - \frac{1}{2\Delta x}(f_{x,i+1} - f_{x,i-1}) = \phi_i, \tag{17}$$

$$\frac{15}{2\Delta x^3}(f_{i+1} - f_{i-1}) - \frac{3}{2\Delta x^2}(f_{x,i+1} + 8f_{x,i} + f_{x,i-1}) = \phi_{x,i}. \tag{18}$$

In the case of $\phi = \sin(k_x x)$ and $k_x = 4\pi$ for $0 \le x \le 1$, we estimate the numerical error by the formula

$$\sigma^2 = \sum_{i=1}^{N}\left(\frac{\sin(k_x x_i)}{k_x^2} - f_i\right)^2,$$

where N is the total grid number and $\Delta x = 1/(N-1)$. The boundary conditions at $x = 0$ ($i = 1$) and $x = 1$ ($i = N$) are $f_1 = f_N = 0$ and $f_{x,1} = f_{x,N} = k_x^{-1}$, respectively. The circles in Fig.2 show the average error σ of the IDO scheme with the center interpolation as a

function of the mesh interval Δx, and it is found that the error has a scaling of Δx^4. As a reference, the results of the finite difference scheme $(f_{i+1}-2f_i+f_{i-1})/\Delta x^2=\phi_i$ are plotted by square dots, and it has Δx^2 scaling. It is understood that the IDO scheme has the spatial accuracy of Δx^4, since f_{xx} derived from the center interpolation uses fine values of the grid without f_{xj} according to eqs.(17). In the expression of f_{xxx}, f_i is not included.

5. Numerical Experiments

5.1 Nonlinear Scalar equation

As examples of nonlinear scalar equation, we examine the shock propagation for Burgers equation and the traveling soliton waves described by the Korteweg-de Vries (KdV) equation[22]. Both the equations has the same form $u_t+uu_x-f(u)=0$. Burgers equation takes $f(u)=\kappa u_{xx}$, where κ is a diffusion coefficient. As is used the same procedure in the previous section, we obtain the higher-order time derivatives by differentiating the governing equation as follows,

$$u_t=-uu_x+\kappa\tilde{u}_{xx}, \tag{19-1}$$

$$u_{tx}=-uu_{xx}-u_x^2+\kappa\tilde{u}_{xxx}, \tag{19-1}$$

$$u_{tt}=-u_tu_x-uu_{tx}+\kappa u_{txx}, \tag{19-2}$$

$$u_{ttx}=-u_{tx}u_x-u_tu_{xx}-u_xu_{tx}-uu_{txx}+\kappa u_{txxx}. \tag{19-3}$$

Here, by using $u_{txx}=-uu_{xxx}-3u_xu_{xx}+\kappa\tilde{u}_{xxxx}$ and $u_{txxx}=-uu_{xxxx}-4u_xu_{xxx}-3u_{xx}^2+\kappa\tilde{u}_{xxxxx}$, the left-hand side terms of eq.(19-2) and (19-3) are fully replaced to spatial derivative terms. We substitute the above equations into the explicit Taylor expansion to do time evolution. We apply the upwind interpolation to the derivative terms derived from the advection term, and the center interpolation to the diffusion term; the derivative terms with the symbol ˜ use the center interpolation, and the other term is the upwind interpolation. In this section, we cut the Taylor expansion up to Δt^2. In order to describe the shock discontinuity, we have added the diffusion term with a small diffusion coefficient, because the IDO scheme is a non-conservative form. The initial condition is the following; $u=a$ for $x<50$ and $u=b$ for $x\geq 50$ at the time t=0. According to the weak solution of the conservation law, the shock speed has $(a+b)/2$. The grid spacing is $\Delta x=1$. When we set $a=1$, $b=-0.5$ and $\kappa=0.3$, the computational result at the time $t=200$ is plotted by the dots in Fig.3. The dashed line indicates the initial state. The shock speed appears to be 0.25 and has good agreement with the weak solution. In the case of lager κ (for example $\kappa=1$), the profile of the shock interface becomes more diffusive, however, the shock speed is same as that of $\kappa=0.3$.

In the case of KdV equation, we replace $\kappa\tilde{u}_{xx}$ term to $-\delta^2\tilde{\tilde{u}}_{xxx}$ and neglect the higher

derivatives more than u_{xx} for the upwind interpolation and more than u_{xxxx} for the center interpolation. The procedure is almost same, and only the difference is to use $\widetilde{\widetilde{u}}_{xxx} = (u_{x,i+1} - 2u_{x,i} + u_{x,i-1})/\Delta x^2$ instead of the center interpolation eq.(2-3) in the following equation,

$$u_t = -uu_x - \delta^2 \widetilde{\widetilde{u}}_{xxx} \tag{20}$$

to keep the stability and conservation for a special case. To check the scheme, we compute the traveling soliton waves. The initial condition is the same as the reference[23], and shown in Fig.4 by the dotted line; $u_i = \cos kx_i$, $u_{x,i} = -k \sin kx_i$, $k = \pi$, $\Delta x = 2.0/N$, $x_i = (i-1)\Delta x$, $N = 192$. The numerical result at t=1.6/π are indicate by the dot dashed line and the result at t=3.6/π is shown by the solid line. It is found that both the results agree well with the results of the reference[23].

5.2. Wave equation

The wave equation described by $f_{tt} - c^2 f_{xx} = 0$ includes both the right traveling wave and left traveling wave. By factorization, we have $(\partial_t - c\partial_x)(\partial_t + c\partial_x)f = 0$ and split this into $f_t + cf_x = g$ and $g_t - cg_x = 0$, where the symbol c is a positive constant. These two equations are easily solved by many numerical schemes, however, it is impossible to factorize multi-dimensional wave equation. The IDO scheme can solve the form $f_{tt} - c^2 f_{xx} = 0$ as it is. According to the Taylor expansion forms (4) and (5), odd order time derivatives are required additionally, so that we use f_t and f_{tx} as new independent variables. Taking time derivative of eqs.(4) and (5), we have the following equations.

$$f^{n+1} = f^n + f_t^n \Delta t + c^2 f_{xx}^n \frac{\Delta t^2}{2} + c^2 f_{xxt}^n \frac{\Delta t^3}{6} + c^4 f_{xxxx}^n \frac{\Delta t^4}{24} + O(\Delta t^5) \tag{21-1}$$

$$f_x^{n+1} = f_x^n + f_{tx}^n \Delta t + c^2 f_{xxx}^n \frac{\Delta t^2}{2} + c^2 f_{txxx}^n \frac{\Delta t^3}{6} + c^4 f_{xxxxx}^n \frac{\Delta t^4}{24} + O(\Delta t^5) \tag{21-2}$$

$$f_t^{n+1} = f_t^n + c^2 f_{xx}^n \Delta t + c^2 f_{txx}^n \frac{\Delta t^2}{2} + c^4 f_{xxxx}^n \frac{\Delta t^3}{6} + c^4 f_{txxxx}^n \frac{\Delta t^4}{24} + O(\Delta t^5) \tag{21-3}$$

$$f_{tx}^{n+1} = f_{tx}^n + c^2 f_{xxx}^n \Delta t + c^2 f_{txxx}^n \frac{\Delta t^2}{2} + c^4 f_{xxxxx}^n \frac{\Delta t^3}{6} + c^4 f_{txxxxx}^n \frac{\Delta t^4}{24} + O(\Delta t^5) \tag{21-4}$$

Deriving the eq.(21-1) - (21-4), we use the relations $f_{tt} = c^2 f_{xx}$ and $f_{tttt} = c^4 f_{xxxx}$, and these spatial derivatives. Since we use the center interpolation of the fifth-order polynomial, higher derivatives than f_{xxxx} are neglected and the time accuracy of this scheme becomes Δt^5 at best. The initial value problem of the wave propagation is examined by means of the above scheme. Figure 5 shows the computational result with c = 1 at t = 50, and the dashed lines indicate the initial profile of f. When we give the initial time derivatives of $f_t = cf_x$ and $f_{tx} = cf_{xx}$, a right traveling wave appears as is

shown in Fig.5(a). The initial conditions of $f_t = -cf_x$ and $f_{tx} = -cf_{xx}$ generate a left traveling wave (Fig.5(c)). In the case of $f_t = 0$ and $f_{tx} = 0$, the profile is split to two waves traveling in both the right and the left directions with the half amplitude (Fig.5(b)). The results are accurate enough for most initial profiles by computing eq.(21), however, a small numerical oscillations appear for the profile with very steep gradients. To smear the oscillation, we add the viscous term $0.2c^2 f_{txx}\Delta t^2$ in eq.(21-3) and $2c^2 f_{txxx}\Delta t^2$ in eq.(21-4) and obtain less diffusive result as is seen in Fig.5.

5.3 1-D Riemann Problem

We consider the Riemann initial value problem for the Euler equations as a more complicated hyperbolic equation. The employed equations for density, velocity and internal energy are as follows,

$$\rho_t = -(\rho u)_x, \tag{22-1}$$

$$u_t = -uu_x - \frac{P_x}{\rho}, \tag{22-2}$$

$$e_t = -ue_x - \frac{P}{\rho}u_x. \tag{22-3}$$

Using these equations, we can derive the set of higher time derivatives $\{\rho_t, \rho_{tt}, \rho_{ttt}, \rho_{tx}, \rho_{ttx}, \rho_{tttx}, \quad u_t, u_{tt}, u_{ttt}, u_{tx}, u_{ttx}, u_{tttx}, e_t, e_{tt}, e_{ttt}, e_{tx}, e_{ttx}, e_{tttx}\}$, whose derivations are shown in APPENDIX. All the independent variables ρ, u, e and these derivatives are defined at the same grid point, and we do not use any staggad grid systems. The initial condition is $\rho = 1$, $P = 1$ for the leftmost 100 zones and $\rho = 0.125$, $P = 0.1$ for the other zones; $u = 0$ and $\gamma = 1.4$ in all zones and $\Delta x = 0.01$. As is mentioned in the section 4, an artificial viscosity q have to be added to the pressure term in order to describe the shock interface. We use a differential form of von Neumann-Richtmyer type [24] $q = \alpha\rho c_s u_x$ (c_s: sound speed) only for the compression region, where the minimum of $u_{x,i-1}$ $u_{x,i}$ and $u_{x,i+1}$ is negative and α is a constant of order of unity. The computational profile of the density is given in Fig.6 by the open circles, and the solid line is the analytic solution. At the contact discontinuity, a small undershoot and overshoot appear as is same with CIP[16,17] and DA-CIP[18]. The sharpness of the shock interface depends on the value α and the computation becomes unstable for $\alpha <$ 0.3

5.4 Two Interacting Blast Waves

For a complicated compressible fluid motion, we examine the test of two interacting blast waves which was reviewed in detail in [5,6,7,9]. The initial condition

consists of three constant states of gamma-law gas with $\gamma = 1.4$; the density is everywhere unity and the pressure is 1000 in the leftmost tenth, 100 in the rightmost, and in between it is 0.01. Both the boundary are reflecting wall separated by a distance of unity. Two strong shock waves develop and collide interacting with rarefaction waves reflected at the boundary. We have used the same scheme as the case of the weak shock problem. The computational mesh used in this calculation is 1/800 uniformly. Figures 7(a) and (b) show the velocity and density profiles at time t=0.016. The density jump has good agreement with conservation law, however small overshoots appear at the contact discontinuity sides. In Figs. 7(c) and (d), the profiles at time t=0.038 are shown. The collision of shock waves produces new contact discontinuities and the density profile becomes quite complicate. The small overshoots which appear in Fig.7(b) still exist at this time. The contours of the density in space-time is shown in Fig.8. Sixty contours are drawn in equally spaced $\log\rho$. Although we use only 800 meshes, the results in Fig.7 and Fig.8 have excellent agreement with the results of [9] with use of 3096 meshes.

6. Conclusion

In this paper, we have presented IDO scheme to solve various kinds of partial differential equations. The independent variables defined at the grid have a spatial profile with the Hermite interpolation which is determined by the values and the first spatial derivatives of the neighboring grids. We use two kinds of the interpolations which have different interpolation areas, and the upwind interpolation is applied only to the advection term. When we use the center interpolation of fifth polynomial to solve Poisson equation, the numerical solution is found to be Δx^4 accuracy. We have applied the IDO scheme to mass continuity equation, and the total mass conservation is kept very well in spite of the non-conservative form. Applications of IDO scheme to nonlinear scalar equation, wave equation and Riemann problem have gone straightforward with the same procedure and excellent results have been obtained. It is concluded that IDO scheme has flexible applicability for hyperbolic, ellipsoidal and parabolic equations and easy to construct the numerical discretization scheme simply by using the given equation.

In the next work, we intend to investigate the numerical stability of the IDO scheme, however we have had stable solutions for all the numerical experiment presented in this paper by choosing Δt.

We have discussed one-dimensional IDO scheme through whole this paper. Because the scheme does not depend on the characteristics, there seems to be no

difficulty to extend IDO scheme to multi-dimensional version if only multi-dimensional interpolation is obtained, and it will be also given in the next paper.

APPENDIX : IDO formulation for Euler equation

We derive the IDO scheme for one-dimensional Euler equation eq.(22) in the explicit form.

$$\rho_t = -\rho_x u - \rho u_x \tag{A-1}$$

$$\rho_{tx} = -\rho_{xx} u - 2\rho_x u_x - \rho u_{xx} \tag{A-2}$$

$$u_t = -uu_x - (p_x + q_x)/\rho \tag{A-3}$$

$$u_{tx} = -u_x^2 - uu_{xx} - (p_{xx} + q_{xx})/\rho + (p_x + q_x)\rho_x/\rho^2 \tag{A-4}$$

$$e_t = -ue_x - (p+q)u_x/\rho \tag{A-5}$$

$$e_{tx} = -u_x e_x - ue_{xx} - (p_x + q_x)u_x/\rho - (p+q)\tilde{u}_{xx}/\rho + (p+q)u_x\rho_x/\rho^2 \tag{A-6}$$

$$\rho_{txx} = -\rho_{xxx} u - 3\rho_{xx} u_x - 3\rho_x u_{xx} - \rho u_{xxx} \tag{A-7}$$

$$\begin{aligned} u_{txx} = {} & -3u_x u_{xx} - uu_{xxx} - (p_{xxx} + q_{xxx})/\rho + 2(p_{xx} + q_{xx})\rho_x/\rho^2 \\ & + (p_x + q_x)\rho_{xx}/\rho^2 - 2(p_x + q_x)\rho_x^2/\rho^3 \end{aligned} \tag{A-8}$$

$$\begin{aligned} e_{txx} = {} & -u_{xx} e_x - 2u_x e_{xx} - ue_{xxx} - (p_{xx} + q_{xx})u_x/\rho \\ & - 2(p_x + q_x)\tilde{u}_{xx}/\rho + 2(p_x + q_x)u_x\rho_x/\rho^2 \\ & - (p+q)\tilde{u}_{xxx}/\rho + 2(p+q)\tilde{u}_{xx}\rho_x/\rho^2 \\ & + (p+q)u_x\tilde{\rho}_{xx}/\rho^2 - 2(p+q)u_x\rho_x^2/\rho^3 \end{aligned} \tag{A-9}$$

The derivatives ρ_{txx}, u_{txx} and e_{txx} are derived in advance, and used to obtain the following higher time derivatives,

$$\rho_{tt} = -\rho_{tx} u - \rho_x u_t - \rho_t u_x - \rho u_{tx} \tag{A-10}$$

$$\rho_{ttx} = -\rho_{txx} u - \rho_{xx} u_t - 2\rho_{tx} u_x - 2\rho_x u_{tx} - \rho_t u_{xx} - \rho u_{txx} \tag{A-11}$$

$$u_{tt} = -u_t u_x - uu_{tx} - (p_{tx} + q_{tx})/\rho + (p_x + q_x)\rho_t/\rho^2 \tag{A-12}$$

$$\begin{aligned} u_{tx} = {} & -2u_{tx} u_x - u_t u_{xx} - uu_{txx} - (p_{txx} + q_{txx})/\rho + (p_{xx} + q_{xx})\rho_t/\rho^2 \\ & + (p_{tx} + q_{tx})\rho_x/\rho^2 + (p_x + q_x)\rho_{tx}/\rho^2 - 2(p_x + q_x)\rho_x\rho_t/\rho^3 \end{aligned} \tag{A-13}$$

$$e_{tt} = -u_t e_x - ue_{tx} - (p_t + q_t)u_x/\rho - (p+q)u_{tx}/\rho + (p+q)u_x\rho_t/\rho^2 \tag{A-14}$$

$$\begin{aligned} e_{ttx} = {} & -u_{tx} e_x - u_x e_{tx} - u_t e_{xx} - ue_{txx} \\ & - (p_{tx} + q_{tx})u_x/\rho - (p_x + q_x)u_{tx}/\rho + (p_x + q_x)u_x\rho_t/\rho^2 \\ & - (p_t + q_t)\tilde{u}_{xx}/\rho - (p+q)u_{txx}/\rho + (p+q)\tilde{u}_{xx}\rho_t/\rho^2 \\ & + (p_t + q_t)u_x\rho_x/\rho^2 + (p+q)u_{tx}\rho_x/\rho^2 \\ & + (p+q)u_x\rho_{tx}/\rho^2 - 2(p+q)u_x\rho_x\rho_t/\rho^3 \end{aligned} \tag{A-15}$$

For ideal equation of state, The pressure p which is a function of ρ and e is written by

$p=(\gamma-1)\rho e$ for the ideal equation of state, and the derivatives are derived as follows,

$$p_x = p_\rho \rho_x + p_e e_x = (\gamma-1)(\rho_x e + \rho e_x), \tag{A-16}$$

$$p_{xx} = (\gamma-1)(\widetilde{\rho}_{xx} e + 2\rho_x e_x + \rho \widetilde{e}_{xx}), \tag{A-17}$$

$$p_{xxx} = (\gamma-1)(\widetilde{\rho}_{xxx} e + 3\widetilde{\rho}_{xx} e_x + 3\rho_x \widetilde{e}_{xx} + \rho \widetilde{e}_{xxx}), \tag{A-18}$$

$$p_{tx} = (\gamma-1)(\rho_{tx} e + \rho_x e_t + \rho_t e_x + \rho e_{tx}), \tag{A-19}$$

$$p_{txx} = (\gamma-1)(\rho_{txx} e + \widetilde{\rho}_{xx} e_t + 2\rho_{tx} e_x + 2\rho_x e_{tx} + \rho_t \widetilde{e}_{xx} + \rho e_{txx}). \tag{A-20}$$

For artificial viscosity, we use the expression $q = \alpha \rho c_s u_x$, and the derivatives are

$$q_x = \alpha c_s(\rho_x u_x + \rho \widetilde{u}_{xx}), \tag{A-21}$$

$$q_{xx} = \alpha c_s(\widetilde{\rho}_{xx} u_x + 2\rho_x \widetilde{u}_{xx} + \rho \widetilde{u}_{xxx}), \tag{A-22}$$

$$q_{xxx} = \alpha c_s(\widetilde{\rho}_{xxx} u_x + 3\widetilde{\rho}_{xx} \widetilde{u}_{xx} + 3\rho_x \widetilde{u}_{xx} + \rho \widetilde{u}_{xxxx}), \tag{A-23}$$

$$q_{tx} = \alpha c_s(\rho_{tx} u_x + \rho_x u_{tx} + \rho_t \widetilde{u}_{xx} + \rho u_{txx}), \tag{A-24}$$

$$q_{txx} = \alpha c_s(\rho_{txx} u_x + \widetilde{\rho}_{xx} u_{tx} + 2\rho_{tx} \widetilde{u}_{xx} + 2\rho_x u_{txx} + \rho_t \widetilde{u}_{xxx} + \rho u_{txxx}), \tag{A-25}$$

where we neglect the dependency of e for the sound speed c_s.

These derivatives are substituted into the following explicit Taylor expansions to update to the time step $t+\Delta t$,

$$\rho^{n+1} = \rho^n + \rho_t^n \Delta t + \tfrac{1}{2}\rho_{tt}^n \Delta t^2, \tag{A-26}$$

$$\rho_x^{n+1} = \rho_x^n + \rho_{tx}^n \Delta t + \tfrac{1}{2}\rho_{ttx}^n \Delta t^2, \tag{A-27}$$

$$u^{n+1} = u^n + u_t^n \Delta t + \tfrac{1}{2} u_{tt}^n \Delta t^2, \tag{A-28}$$

$$u_x^{n+1} = u_x^n + u_{tx}^n \Delta t + \tfrac{1}{2} u_{ttx}^n \Delta t^2, \tag{A-29}$$

$$e^{n+1} = e^n + e_t^n \Delta t + \tfrac{1}{2} e_{tt}^n \Delta t^2, \tag{A-30}$$

$$e_x^{n+1} = e_x^n + e_{tx}^n \Delta t + \tfrac{1}{2} e_{ttx}^n \Delta t^2. \tag{A-31}$$

The time accuracy of Δt^2 is enough for the CFL number less than 0.2. In the above equations, the derivatives with the symbol tilde come from the center interpolation for equal to or higher than second derivative, the derivatives without tilde come from the upwind derivative.

Acknowledgments

The author would like to thank Prof. Yabe for the useful comment and his encouragement. This work was carried out under the collaborating research program at the National Institute for Fusion Science of Japan.

References

[1] A. Harten, J. Comput. Phys. **49** (1983) 357.

[2] H. Yang, J. Comput. Phys. **89** (1990) 125.

[3] S. Osher and S. Chakravarthy, SIAM *J. Numer. Anal.*, **21** (1984) 955.

[4] A. Harten, J. Comput. Phys. **71** (1987) 231.

[5] A. Harten, J. Comput. Phys. **83** (1989) 148.
[6] C-W. Shu and S. Osher, J. Comput. Phys. **83** (1989) 32.
[7] H. Nessyahu and E. Tadmor, J. Comput. Phys. **87** (1990) 408.
[8] P. Colella and P. R. Woodward, J. Comput. Phys. **54** (1984) 174.
[9] P. Woodward and P. Colella, J. Comput. Phys. **54** (1984) 115.
[10] S. Karni, J. Comput. Phys., **112** (1994) 31.
[11] H. Takewaki, A. Nishiguchi and T. Yabe, J. Comput. Phys. **61** (1985) 261.
[12] H. Yakewaki and T. Yabe, J. Comput. Phys. **70** (1987) 355.
[13] T. Yabe, Rev. Laser Eng., **20** (1992) 691.
[14] T. Yabe and F. Xiao, J. Phys. Soc. Jpn. **62** (1993) 2537.
[15] T. Yabe , et al., Geophys. Res. Lett., **22** (1995) 2429.
[16] T. Yabe and E. Takei, J. Phys. Soc. Jpn. **57** (1988) 2598.
[17] T. Yabe and T. Aoki, Comput. Phys. Commun. **66** (1991) 219.
[18] T. Utsumi, Comput. Fluid Dynamics J. **4** (1995) 225.
[19] Y. Kondoh, Y. Hosaka and K. Ishii, Comput. Math. Applic. **27** (1994) 59
[20] F. Xiao, T. Yabe, G. Nizam and T. Itoh, Comput. Phys. Commun. **93** (1996) 1.
[21] M. Ida and T. Yabe, Comput. Phys. Commun. **92** (1995) 21.
[22] D. J. Korteweg and de Vries, Philos. Mag. Ser. **5** (1895) 422.
[23] N. J. Zabusky and M. D. Kruskal, Phys. Rev. Lett., **15** (1965) 240.
[24] J. von Neumann and R. D. Richtmyer, J. Appl. Phys. **21** (1950) 232.

Figure Captions

Fig.1. Mass Conservation as a function of velocity nonuniformity k_x, where the velocity profile is $u = 1 + 0.25\sin(k_x x)$. The solid line indicates the result of the IDO after 500 steps with $\Delta t = 0.4$ and $\Delta x = 1$. The dashed line shows the result of 3rd order upwind FDM of non-conservative form.

Fig.2. Spatial accuracy of the numerical solution for Poisson equation by using IDO scheme. The solid circles represent the computational result of IDO scheme showing Δx^4 accuracy, and the solid triangles show Δx^2 accuracy for the result of the center finite difference method $(f_{i+1} - 2f_i + f_{i-1}) / \Delta x^2 = \phi_i$.

Fig.3. The profiles of the numerical solution of the Burgers equation at $t = 200$. The initial profile is indicated by the dashed line. The speed of shock front is found

to be 0.25.

Fig.4. The numerical results of the KdV equation with $\Delta x = 1/192$. The dashed line is the initial profile. The dot dashed line is the profile of $t = 1/\pi$, and the solid line shows that of $t = 3.6/\pi$.

Fig.5. The results of wave equation by using IDO with the center interpolation. The dashed lines show the initial profile. When the initial conditions of the first time derivative are $f_t = cf_x$ and $f_t = -cf_x$, the results show left traveling wave (a) and right traveling wave (c), respectively. When the initial time derivative is zero, the profile is split into two waves (b).

Fig.6. The results of applying IDO scheme to Riemann problem. The initial profile is $\rho = 1, u = 0, P = 1$ for $x < 1$ and $\rho = 0.125, u = 0, P = 0.1$ for $x \geq 1$. The solid line shows the analytic solution, and the open circles denote the computational result of the density profile.

Fig.7. The interaction of two blast waves are computed by IDO scheme with a uniform grid of 800 zones. The velocity (a) and density (b) profiles of $t = 0.016$ are shown in the upper half, and those of $t = 0.038$ are in the lower half.

Fig.8. Contours of density on the space-time plane for the interacting blast wave problem. Sixty contours equally spaced in $\log \rho$ are shown.

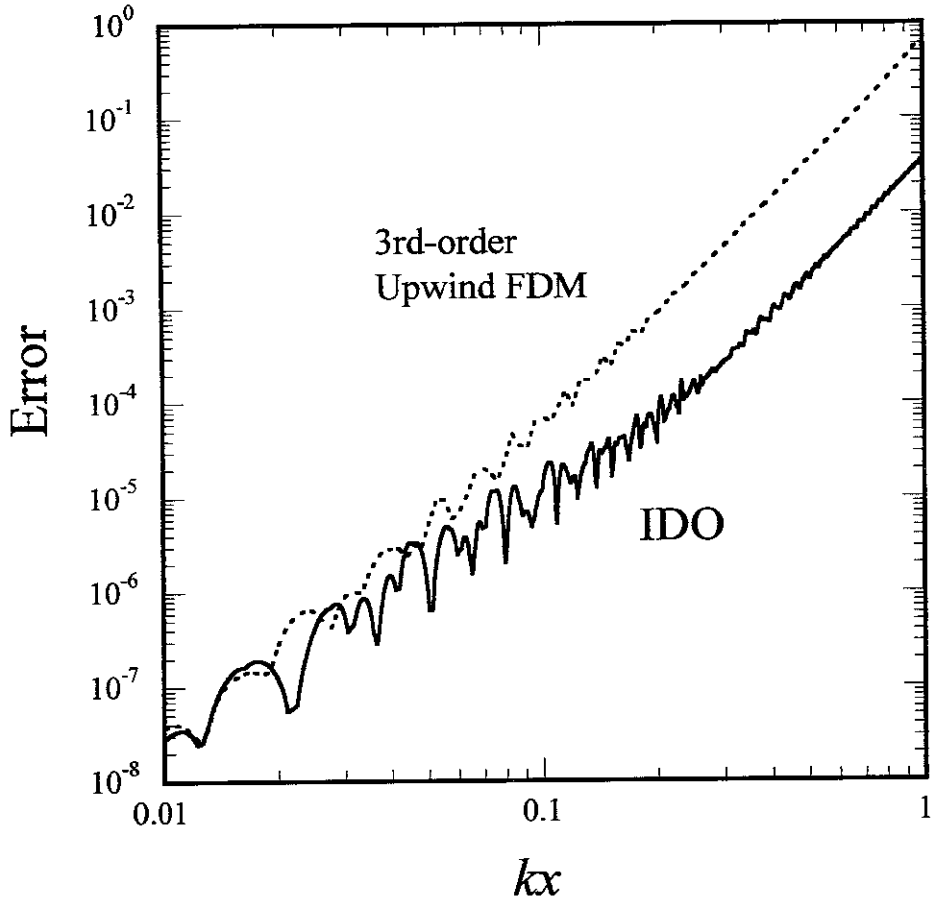

Fig.1. Mass Conservation as a function of velocity nonuniformity k_x, where the velocity profile is $u = 1 + 0.25\sin(k_x x)$. The solid line indicates the result of the IDO after 500 steps with $\Delta t = 0.4$ and $\Delta x = 1$. The dashed line shows the result of 3rd order upwind FDM of non-conservative form.

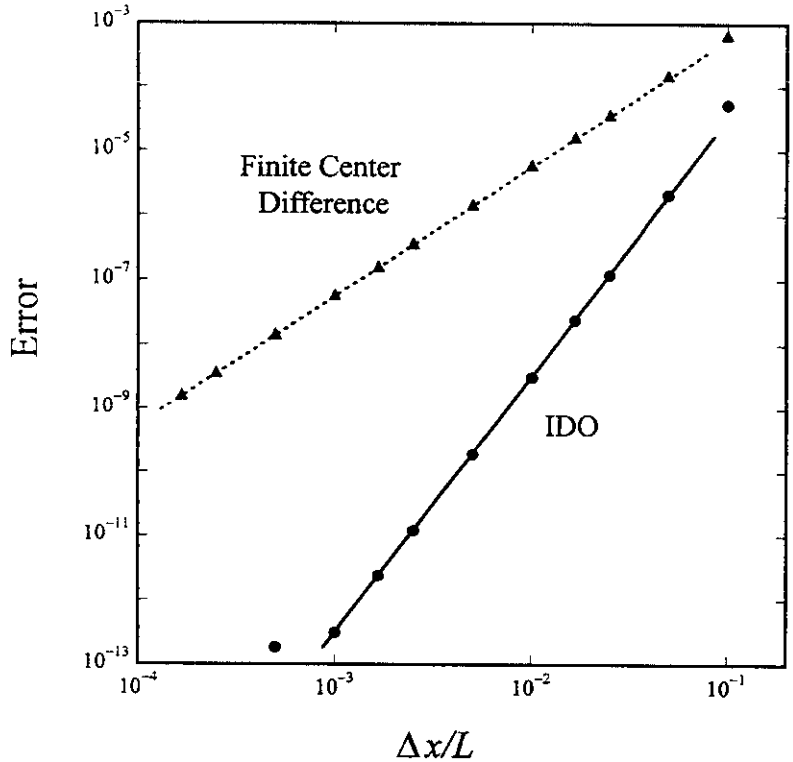

Fig.2. Spatial accuracy of the numerical solution for Poisson equation by using IDO scheme. The solid circles represent the computational result of IDO scheme showing Δx^4 accuracy, and the solid triangles show Δx^2 accuracy for the result of the center finite difference method $(f_{i+1} - 2f_i + f_{i-1}) / \Delta x^2 = \phi_i$.

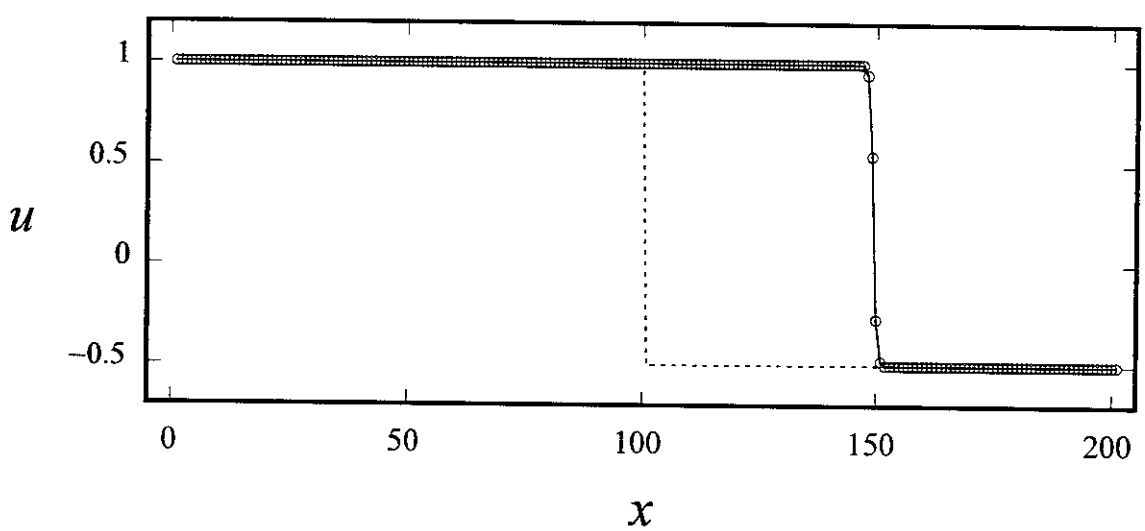

Fig.3. The profiles of the numerical solution of the Burgers equation at $t = 200$. The initial profile is indicated by the dashed line. The speed of shock front is found to be 0.25.

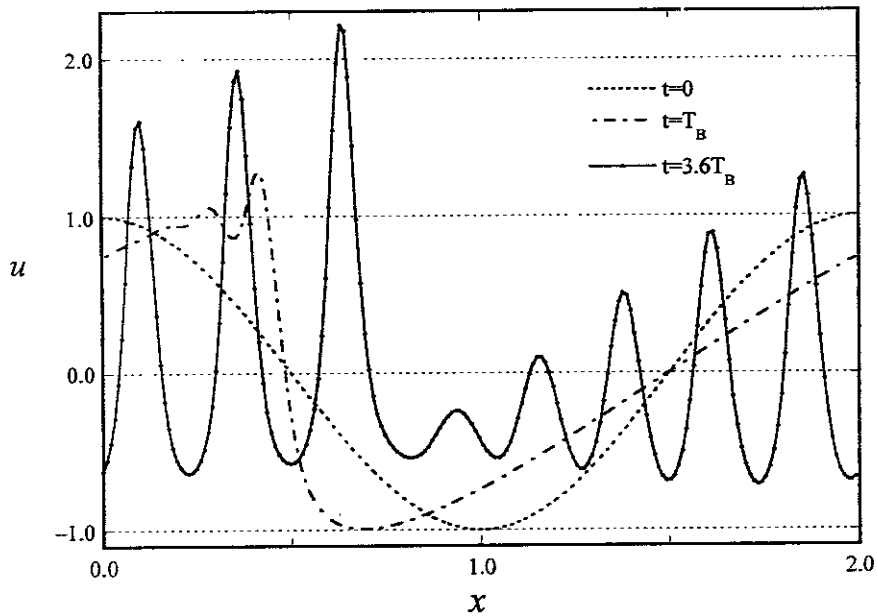

Fig.4. The numerical results of the KdV equation with $\Delta x = 1/192$. The dashed line is the initial profile. The dot dashed line is the profile of $t = 1/\pi$, and the solid line shows that of $t = 3.6/\pi$.

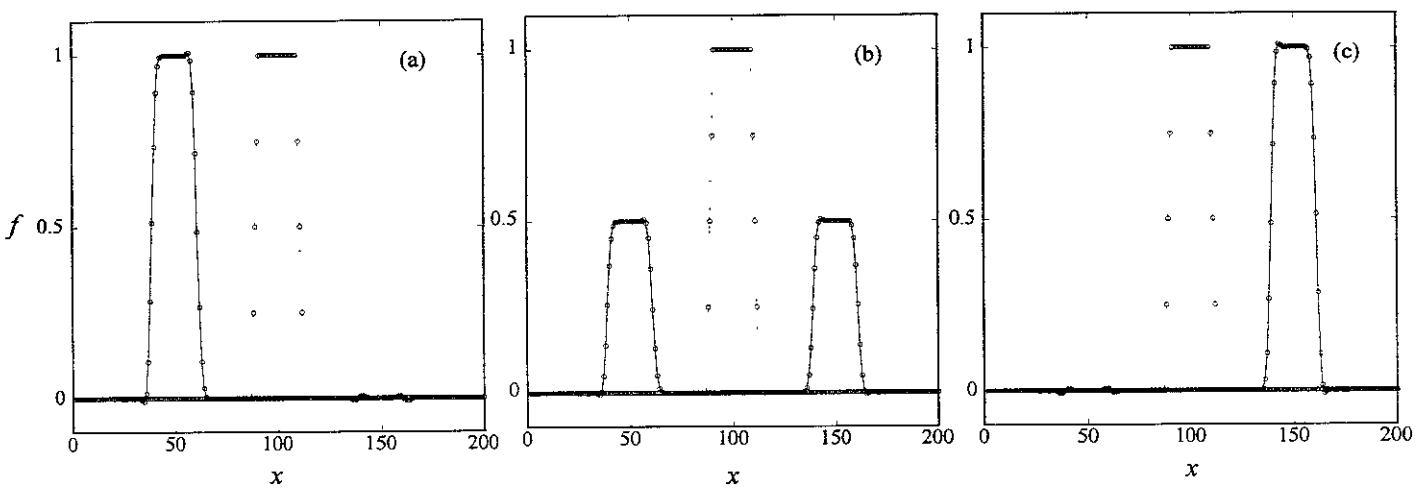

Fig.5. The results of wave equation by using IDO with the center interpolation. The dashed lines show the initial profile. When the initial conditions of the first time derivative are $f_t = cf_x$ and $f_t = -cf_x$, the results show left traveling wave (a) and right traveling wave (c), respectively. When the initial time derivative is zero, the profile is split into two waves (b).

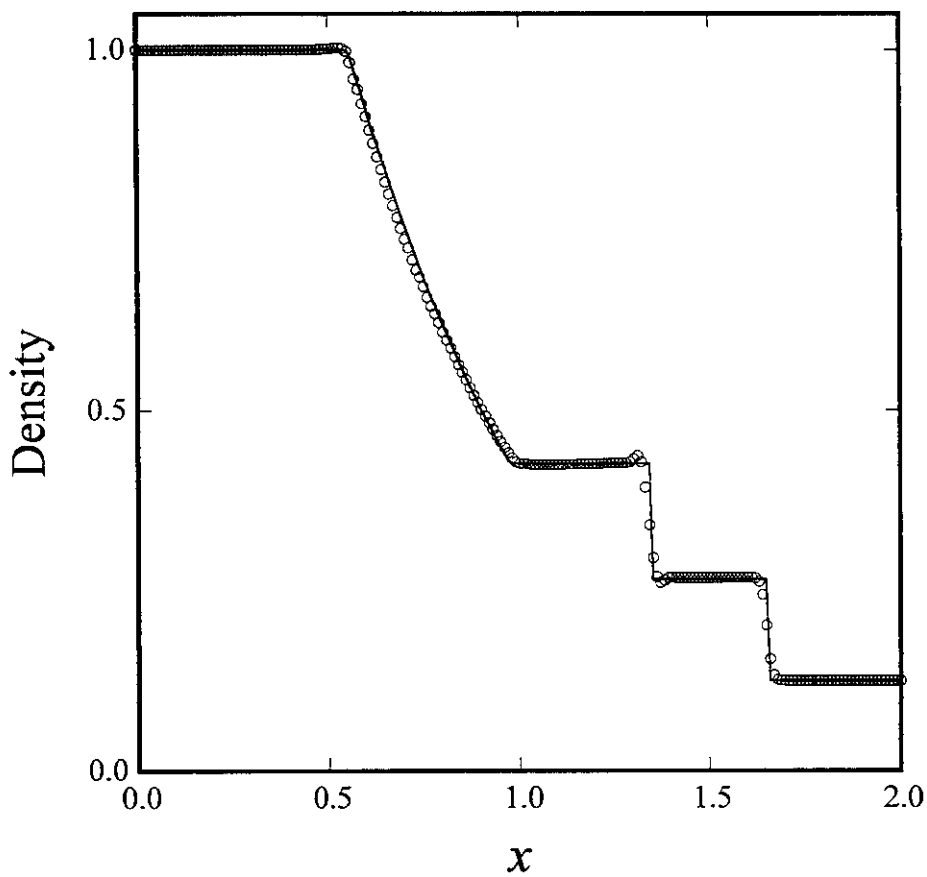

Fig.6. The results of applying IDO scheme to Riemann problem. The initial profile is $\rho = 1$, $u = 0$, $P = 1$ for $x < 1$ and $\rho = 0.125$, $u = 0$, $P = 0.1$ for $x \geq 1$. The solid line shows the analytic solution, and the open circles denote the computational result of the density profile.

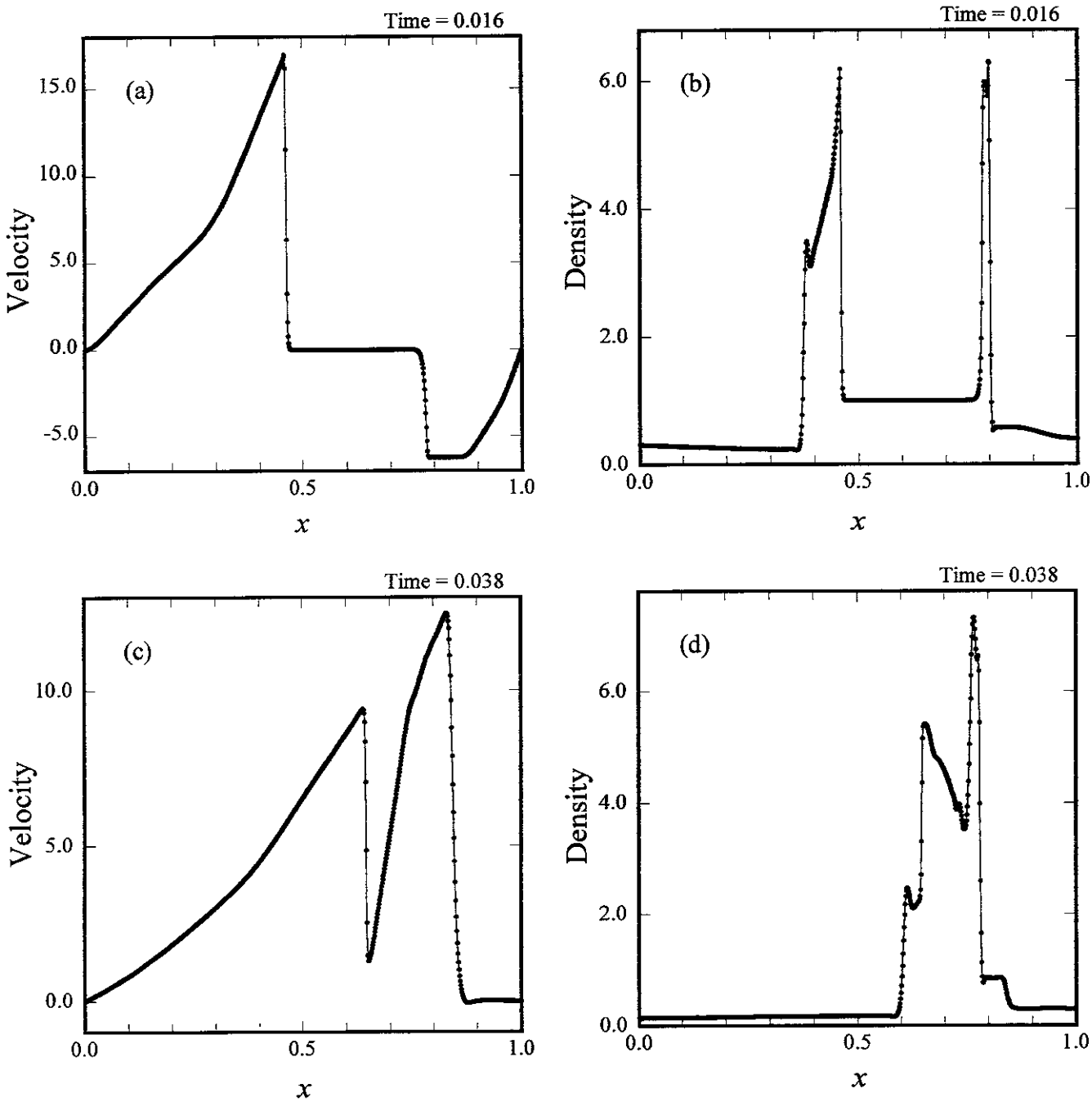

Fig.7. The interaction of two blast waves are computed by IDO scheme with a uniform grid of 800 zones. The velocity (a) and density (b) profiles of $t = 0.016$ are shown in the upper half, and those of $t = 0.038$ are in the lower half.

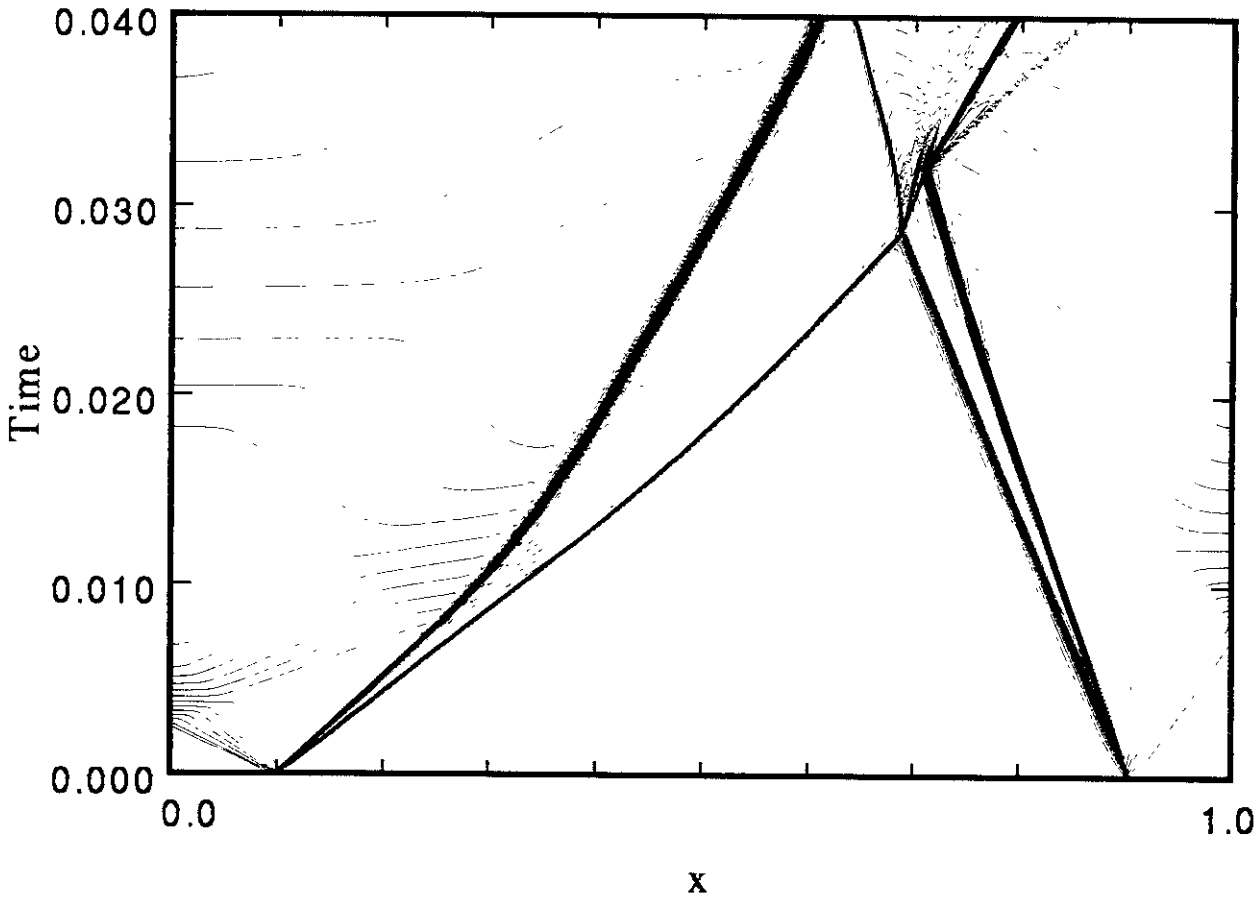

Fig.8. Contours of density on the space-time plane for the interacting blast wave problem. Sixty contours equally spaced in $\log \rho$ are shown.

Recent Issues of NIFS Series

NIFS-413 Y. Nomura, Y.H. Ichikawa and A.T. Filippov,
Stochasticity in the Josephson Map; Apr. 1996

NIFS-414 J. Uramoto,
Production Mechanism of Negative Pionlike Particles in H_2 Gas Discharge Plasma; Apr. 1996

NIFS-415 A. Fujisawa, H. Iguchi, S. Lee, T.P. Crowley, Y. Hamada, S. Hidekuma, M. Kojima,
Active Trajectory Control for a Heavy Ion Beam Probe on the Compact Helical System; May 1996

NIFS-416 M. Iwase, K. Ohkubo, S. Kubo and H. Idei
Band Rejection Filter for Measurement of Electron Cyclotron Emission during Electron Cyclotron Heating; May 1996

NIFS-417 T. Yabe, H. Daido,T. Aoki, E. Matsunaga and K. Arisawa,
Anomalous Crater Formation in Pulsed-Laser-Illuminated Aluminum Slab and Debris Distribution; May 1996

NIFS-418 J. Uramoto,
Extraction of K^- Mesonlike Particles from a D_2 Gas Discharge Plasma in Magnetic Field; May 1996

NIFS-419 J. Xu, K. Toi, H. Kuramoto, A. Nishizawa, J. Fujita, A. Ejiri, K. Narihara, T. Seki, H. Sakakita, K. Kawahata, K. Ida, K. Adachi, R. Akiyama, Y. Hamada, S. Hirokura, Y. Kawasumi, M. Kojima, I. Nomura, S. Ohdachi, K.N. Sato
Measurement of Internal Magnetic Field with Motional Stark Polarimetry in Current Ramp-Up Experiments of JIPP T-IIU; June 1996

NIFS-420 Y.N. Nejoh,
Arbitrary Amplitude Ion-acoustic Waves in a Relativistic Electron-beam Plasma System; July 1996

NIFS-421 K. Kondo, K. Ida, C. Christou, V.Yu.Sergeev, K.V.Khlopenkov, S.Sudo, F. Sano, H. Zushi, T. Mizuuchi, S. Besshou, H. Okada, K. Nagasaki, K. Sakamoto, Y. Kurimoto, H. Funaba, T. Hamada, T. Kinoshita, S. Kado, Y. Kanda, T. Okamoto, M. Wakatani and T. Obiki,
Behavior of Pellet Injected Li Ions into Heliotron E Plasmas; July 1996

NIFS-422 Y. Kondoh, M. Yamaguchi and K. Yokozuka,
Simulations of Toroidal Current Drive without External Magnetic Helicity Injection; July 1996

NIFS-423 Joong-San Koog,

Development of an Imaging VUV Monochromator in Normal Incidence Region; July 1996

NIFS-424 K. Orito,
A New Technique Based on the Transformation of Variables for Nonlinear Drift and Rossby Vortices; July 1996

NIFS-425 A. Fujisawa, H. Iguchi, S. Lee, T.P. Crowley, Y. Hamada, H. Sanuki, K. Itoh, S. Kubo, H. Idei, T. Minami, K. Tanaka, K. Ida, S. Nishimura, S. Hidekuma, M. Kojima, C. Takahashi, S. Okamura and K. Matsuoka,
Direct Observation of Potential Profiles with a 200keV Heavy Ion Beam Probe and Evaluation of Loss Cone Structure in Toroidal Helical Plasmas on the Compact Helical System; July 1996

NIFS-426 H. Kitauchi, K. Araki and S. Kida,
Flow Structure of Thermal Convection in a Rotating Spherical Shell; July 1996

NIFS-427 S. Kida and S. Goto,
Lagrangian Direct-interaction Approximation for Homogeneous Isotropic Turbulence; July 1996

NIFS-428 V.Yu. Sergeev, K.V. Khlopenkov, B.V. Kuteev, S. Sudo, K. Kondo, F. Sano, H. Zushi, H. Okada, S. Besshou, T. Mizuuchi, K. Nagasaki, Y. Kurimoto and T. Obiki,
Recent Experiments on Li Pellet Injection into Heliotron E; Aug. 1996

NIFS-429 N. Noda, V. Philipps and R. Neu,
A Review of Recent Experiments on W and High Z Materials as Plasma-Facing Components in Magnetic Fusion Devices; Aug. 1996

NIFS-430 R.L. Tobler, A. Nishimura and J. Yamamoto,
Design-Relevant Mechanical Properties of 316-Type Stainless Steels for Superconducting Magnets; Aug. 1996

NIFS-431 K. Tsuzuki, M. Natsir, N. Inoue, A. Sagara, N. Noda, O. Motojima, T. Mochizuki, T. Hino and T. Yamashina,
Hydrogen Absorption Behavior into Boron Films by Glow Discharges in Hydrogen and Helium; Aug. 1996

NIFS-432 T.-H. Watanabe, T. Sato and T. Hayashi,
Magnetohydrodynamic Simulation on Co- and Counter-helicity Merging of Spheromaks and Driven Magnetic Reconnection; Aug. 1996

NIFS-433 R. Horiuchi and T. Sato,
Particle Simulation Study of Collisionless Driven Reconnection in a Sheared Magnetic Field; Aug. 1996

NIFS-434 Y. Suzuki, K. Kusano and K. Nishikawa,
Three-Dimensional Simulation Study of the Magnetohydrodynamic Relaxation Process in the Solar Corona. II.; Aug. 1996

NIFS-435 H. Sugama and W. Horton,
Transport Processes and Entropy Production in Toroidally Rotating Plasmas with Electrostatic Turbulence; Aug. 1996

NIFS-436 T. Kato, E. Rachlew-Källne, P. Hörling and K.-D Zastrow,
Observations and Modelling of Line Intensity Ratios of OV Multiplet Lines for 2s3s 3S1 - 2s3p 3Pj; Aug. 1996

NIFS-437 T. Morisaki, A. Komori, R. Akiyama, H. Idei, H. Iguchi, N. Inoue, Y. Kawai, S. Kubo, S. Masuzaki, K. Matsuoka, T. Minami, S. Morita, N. Noda, N. Ohyabu, S. Okamura, M. Osakabe, H. Suzuki, K. Tanaka, C. Takahashi, H. Yamada, I. Yamada and O. Motojima,
Experimental Study of Edge Plasma Structure in Various Discharges on Compact Helical System; Aug. 1996

NIFS-438 A. Komori, N. Ohyabu, S. Masuzaki, T. Morisaki, H. Suzuki, C. Takahashi, S. Sakakibara, K. Watanabe, T. Watanabe, T. Minami, S. Morita, K. Tanaka, S. Ohdachi, S. Kubo, N. Inoue, H. Yamada, K. Nishimura, S. Okamura, K. Matsuoka, O. Motojima, M. Fujiwara, A. Iiyoshi, C. C. Klepper, J.F. Lyon, A.C. England, D.E. Greenwood, D.K. Lee, D.R. Overbey, J.A. Rome, D.E. Schechter and C.T. Wilson,
Edge Plasma Control by a Local Island Divertor in the Compact Helical System; Sep. 1996 (IAEA-CN-64/C1-2)

NIFS-439 K. Ida, K. Kondo, K. Nagaski T. Hamada, H. Zushi, S. Hidekuma, F. Sano, T. Mizuuchi, H. Okada, S. Besshou, H. Funaba, Y. Kurimoto, K. Watanabe and T. Obiki,
Dynamics of Ion Temperature in Heliotron-E; Sep. 1996 (IAEA-CN-64/CP-5)

NIFS-440 S. Morita, H. Idei, H. Iguchi, S. Kubo, K. Matsuoka, T. Minami, S. Okamura, T. Ozaki, K. Tanaka, K. Toi, R. Akiyama, A. Ejiri, A. Fujisawa, M. Fujiwara, M. Goto, K. Ida, N. Inoue, A. Komori, R. Kumazawa, S. Masuzaki, T. Morisaki, S. Muto, K. Narihara, K. Nishimura, I. Nomura, S. Ohdachi, M.. Osakabe, A. Sagara, Y. Shirai, H. Suzuki, C. Takahashi, K. Tsumori, T. Watari, H. Yamada and I. Yamada,
A Study on Density Profile and Density Limit of NBI Plasmas in CHS; Sep. 1996 (IAEA-CN-64/CP-3)

NIFS-441 O. Kaneko, Y. Takeiri, K. Tsumori, Y. Oka, M. Osakabe, R. Akiyama, T. Kawamoto, E. Asano and T. Kuroda,
Development of Negative-Ion-Based Neutral Beam Injector for the Large Helical Device; Sep. 1996 (IAEA-CN-64/GP-9)

NIFS-442 K. Toi, K.N. Sato, Y. Hamada, S. Ohdachi, H. Sakakita, A. Nishizawa, A. Ejiri, K.

Narihara, H. Kuramoto, Y. Kawasumi, S. Kubo, T. Seki, K. Kitachi, J. Xu, K. Ida, K. Kawahata, I. Nomura, K. Adachi, R. Akiyama, A. Fujisawa, J. Fujita, N. Hiraki, S. Hidekuma, S. Hirokura, H. Idei, T. Ido, H. Iguchi, K. Iwasaki, M. Isobe, O. Kaneko, Y. Kano, M. Kojima, J. Koog, R. Kumazawa, T. Kuroda, J. Li, R. Liang, T. Minami, S. Morita, K. Ohkubo, Y. Oka, S. Okajima, M. Osakabe, Y. Sakawa, M. Sasao, K. Sato, T. Shimpo, T. Shoji, H. Sugai, T. Watari, I. Yamada and K. Yamauti,
Studies of Perturbative Plasma Transport, Ice Pellet Ablation and Sawtooth Phenomena in the JIPP T-IIU Tokamak; Sep. 1996 (IAEA-CN-64/A6-5)

NIFS-443 Y. Todo, T. Sato and The Complexity Simulation Group,
Vlasov-MHD and Particle-MHD Simulations of the Toroidal Alfvén Eigenmode; Sep. 1996 (IAEA-CN-64/D2-3)

NIFS-444 A. Fujisawa, S. Kubo, H. Iguchi, H. Idei, T. Minami, H. Sanuki, K. Itoh, S. Okamura, K. Matsuoka, K. Tanaka, S. Lee, M. Kojima, T.P. Crowley, Y. Hamada, M. Iwase, H. Nagasaki, H. Suzuki, N. Inoue, R. Akiyama, M. Osakabe, S. Morita, C. Takahashi, S. Muto, A. Ejiri, K. Ida, S. Nishimura, K. Narihara, I. Yamada, K. Toi, S. Ohdachi, T. Ozaki, A. Komori, K. Nishimura, S. Hidekuma, K. Ohkubo, D.A. Rasmussen, J.B. Wilgen, M. Murakami, T. Watari and M. Fujiwara,
An Experimental Study of Plasma Confinement and Heating Efficiency through the Potential Profile Measurements with a Heavy Ion Beam Probe in the Compact Helical System; Sep. 1996 (IAEA-CN-64/C1-5)

NIFS-445 O. Motojima, N. Yanagi, S. Imagawa, K. Takahata, S. Yamada, A. Iwamoto, H. Chikaraishi, S. Kitagawa, R. Maekawa, S. Masuzaki, T. Mito, T. Morisaki, A. Nishimura, S. Sakakibara, S. Satoh, T. Satow, H. Tamura, S. Tanahashi, K. Watanabe, S. Yamaguchi, J. Yamamoto, M.Fujiwara and A. Iiyoshi,
Superconducting Magnet Design and Construction of LHD; Sep. 1996 (IAEA-CN-64/G2-4)

NIFS-446 S. Murakami, N. Nakajima, S. Okamura, M. Okamoto and U. Gasparino,
Orbit Effects of Energetic Particles on the Reachable β–Value and the Radial Electric Field in NBI and ECR Heated Heliotron Plasmas; Sep. 1996 (IAEA-CN-64/CP -6) Sep. 1996

NIFS-447 K. Yamazaki, A. Sagara, O. Motojima, M. Fujiwara, T. Amano, H. Chikaraishi, S. Imagawa, T. Muroga, N. Noda, N. Ohyabu, T. Satow, J.F. Wang, K.Y. Watanabe, J. Yamamoto , H. Yamanishi, A. Kohyama, H. Matsui, O. Mitarai, T. Noda, A.A. Shishkin, S. Tanaka and T. Terai
Design Assessment of Heliotron Reactor; Sep. 1996 (IAEA-CN-64/G1-5)

NIFS-448 M. Ozaki, T. Sato and the Complexity Simulation Group,
Interactions of Convecting Magnetic Loops and Arcades; Sep. 1996

NIFS-449 T. Aoki,
Interpolated Differential Operator (IDO) Scheme for Solving Partial Differential Equations; Sep. 1996